



Preparation of dual-shell Si/TiO₂/CFs composite and its lithium storage performance

Jing ZENG^{1,2}, Chao-qun PENG¹, Ri-chu WANG^{1,2}, Ya-jing LIU^{1,2}, Xiao-feng WANG^{1,2}, Jun LIU¹

1. School of Materials Science and Engineering, Central South University, Changsha 410083, China;

2. Hunan Provincial Key Laboratory of Electronic Packaging and Advanced Functional Materials, Changsha 410083, China

Received 22 April 2019; accepted 27 September 2019

Abstract: A dual-shell Si/TiO₂/CFs composite was synthesized through a simple method to deal with the intrinsic drawbacks of silicon-based anode, in terms of huge volume change, unstable SEI films, and low electronic and ionic conductivity. The inner rigid TiO₂ shell alleviates the huge volume expansion of the nano silicon, and the outer resilient carbon fiber, which is porous and staggered, is beneficial to the rapid transport of electrons and ions. The as-prepared Si/TiO₂/CFs composite displays a superior reversible specific capacity of 583.4 mA·h/g, high rate capability and decent cycling performance. The dual-shell encapsulation method provides a guideline for other anode materials with huge volume expansion during the cycling process.

Key words: dual-shell; Si-based anode; electrospinning; sol-gel method; lithium-ion batteries

1 Introduction

Developing sustainable energy is one of the most effective approaches to tackle the fossil energy crisis and global environmental pollution. Among them, lithium-ion batteries are often utilized in portable electronic equipment such as electric vehicles, laptops, and mobile phones because of their long cycle life and high energy density [1,2]. However, commercial graphite anode is not suitable for next generation lithium-ion batteries, for its relatively low theoretical specific capacity (372 mA·h/g) [3]. Hence, finding new anode materials with higher energy density and economic benefits to satisfy the demands of hybrid electric vehicles, smart grid and other large-scale power equipment is very urgent [4].

Silicon is a potential candidate anode material for lithium storage because of its superior theoretical capacity of 4200 mA·h/g and suitable lithiation voltage platform, which can avoid the generation of lithium dendrites and alleviate the safety problem of electrode materials [5]. Unfortunately, the development and

commercial application of silicon-based materials still suffer from their intrinsic drawbacks [6]. Firstly, silicon is a semiconductor material with extremely low electronic conductivity and ionic conductivity, leading to sluggish electrochemical kinetics [7]. Secondly, the volume expansion of silicon is as high as 400% during the charge–discharge process, resulting in the irreversible breakage and pulverization of electrode material [8]. In addition, the continuous break and generation of unstable SEI film caused by the repeated volume expansion and contraction of silicon-based materials, eventually contribute to a large capacity decay [9].

In recent years, designing nanostructures, such as nanoparticles, hollow or porous characteristics, has been devoted to obtain higher specific capacity, rate performance and cycle life of silicon-based anodes than that of bulk ones [10–12]. However, it is still difficult for silicon-based anodes to achieve long-term cycling stability owing to the insufficient space for accommodating the huge volume expansion, uncontrollable growth of SEI film, and inevitable side effects [13]. The surface coating strategy is a straight-

Foundation item: Project (51772331) supported by the National Natural Science Foundation of China; Project (2018YFB1106000) supported by the National Key Technologies R&D Program of China

Corresponding author: Xiao-feng WANG, Tel: +86-13467516329, E-mail: wangxiaofeng@csu.edu.cn;

Jun LIU, Tel: +86-15802608591, E-mail: liujun4982004@csu.edu.cn

DOI: 10.1016/S1003-6326(19)65144-7

forward way to isolate the direct contact between the electrolyte and Si, buffer the stress change, and also provide a fast transport channel for Li^+ [14]. In this context, a series of coating materials, including intrinsic oxide layer (SiO_2 , SiO_x), carbon-based materials (citric acid, PVDF, graphene), metals (Cu, Ag, Fe), metal oxides (TiO_2 , Al_2O_3), and conductive polymers (polyaniline, polypyrrole) have been introduced into silicon nanostructures [6,15–17]. WU et al [18] grew a uniform silicon layer on the polymer template via a CVD method, then selectively removed the internal carbon template and oxidized the silicon surface, thereby forming a hollow@Si@ SiO_2 nanotube structure, which effectively maintained the stability of the SEI film. FANG et al [14] used rigid TiO_2 to encapsulate silicon nanoparticles, and then etched silicon oxide on the surface of silicon nanoparticles to form Si@hollow@ TiO_2 structure. However, such unique architectures require a sophisticated synthesis process accompanied by the use of hazardous acid, and also reduce the mechanical stability [19]. Therefore, it is immensely challenging to explore a simple method to generate silicon-based materials with stable cycling performance as well as high compact density.

Here, we introduced dual shells, i.e. a rigid (TiO_2) shell and a resilient (carbon fiber) shell to prepare silicon-based anode materials with high mechanical strength, high conductivity, and high uniformity. The rigid TiO_2 with a volume expansion of only 4% can effectively relieve the violent volume change of nano silicon during the cycling process. Electrospinning carbon fiber was utilized to achieve the uniform distribution of the Si/ TiO_2 composite and improve the conductivity of electrode materials. Under the synergistic effect of the three components, the Si/ TiO_2 /CFs composite shows excellent structural stability and electrochemical properties.

2 Experimental

2.1 Synthesis of Si/ TiO_2 core-shell structure

A simple sol-gel method was used to encapsulate the Si nanoparticles. In a typical procedure, 0.45 g of Si nanoparticles with a particle size of 30–50 nm was added into a mixed solution containing 600 mL of absolute ethanol and 0.9 mL of ammonium hydroxide under ultrasonic for 30 min and stirred at 40 °C for 30 min. And then, 2 mL of titanium isopropylate was dropwise added into the mixture and the mixture was kept at 40 °C under gentle magnetic stirring (200 r/min) for 40 h. The Si/ TiO_2 core-shell composite was collected after washing by water and absolute ethanol three times and drying under 80 °C for 24 h.

2.2 Synthesis of Si/ TiO_2 /CFs composite

The Si/ TiO_2 /CFs composite was synthesized through an electrospinning process as illustrated in Fig. 1. Firstly, polyacrylonitrile (PAN, $M_w=150000$) was dissolved in *N,N'*-dimethylformamide (DMF, 99.8%) under vigorous magnetic stirring to form a uniform, transparent, and bubble-free PAN solutions (10 wt.%). Then, the Si/ TiO_2 composite was put into the PAN solutions under magnetic stirring for 24 h and ultrasonic treatment for 1 h to obtain homogeneous suspensions (mass ratio of composite to PAN is 1:4). Thirdly, the suspension was held for 0.5 h to exclude bubbles before being sucked into the syringe. The electrospinning was carried out on a home-made electrospinning device with a spinning speed of 1 mL/h, applied voltage of 25 V, and receiving distance of 20 cm. After spinning, the fresh fibers were stabilized at 250 °C for 2 h in air with a heating rate of 1 °C/min, and then carbonized at 800 °C for 2 h in N_2 atmosphere with a ramp rate of 10 °C/min. For reference, silicon nanoparticles without TiO_2 surface

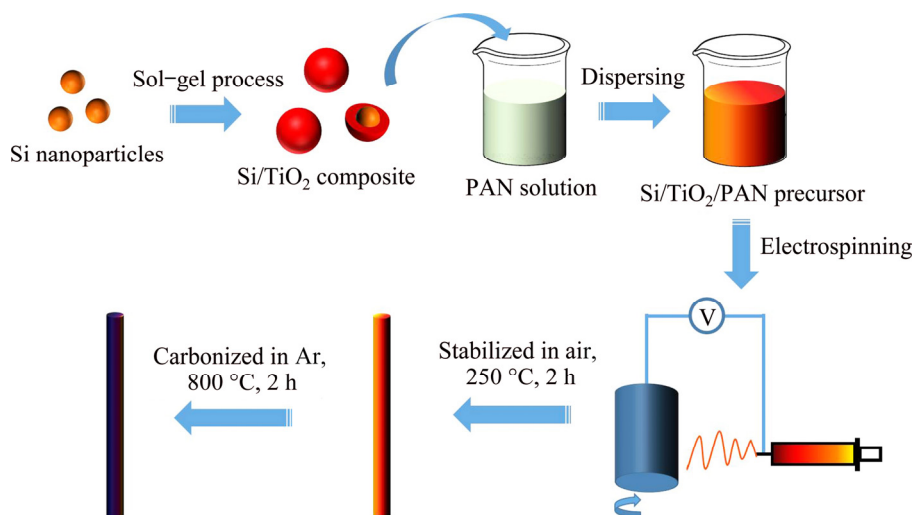


Fig. 1 Schematic diagram of preparation of Si/ TiO_2 /CFs composite

modification were also prepared into Si/CFs composite by the same method.

2.3 Materials characterization

X-ray diffraction (XRD) patterns were obtained on a Rigaku D/max 2500 using Cu K_{α} radiation ($\lambda=0.15405$ nm) scanning with 2θ of 10° – 80° at a sweep speed of 8° /min. Raman spectrum was detected using a LabRAM HR 800 Raman spectrometer (HORIBA Jobin Yvon, France) in a scanning range of 100 – 500 cm^{-1} . The surface and cross-section morphologies were determined using a scanning electron microscope (SEM, Nano SEM 230, FEI, America). Thermal gravimetric analysis (TGA, STA449F3, NETZSCH, Germany) was used to detect the content of every component with a heating rate of $10^{\circ}\text{C}/\text{min}$ in air. And the crystal structures of micro-sized composite were collected using a transmission electron microscope (TEM, Tecnai G2 F20, FEI, America).

2.4 Electrochemical tests

CR2016 coin cells were assembled and used for electrochemical experiment. The Si/TiO₂/CFs composite, acetylene black, and polyacrylic acid (PAA) were used as active material, conductive agent, and binder, respectively at a mass ratio of 7:2:1. Then, the slurry was

pasted on a copper foil and dried in a vacuum oven at 110°C for 12 h. The electrolyte consists of ethylene carbonate (EC)/diethyl carbonate (DEC)/dimethyl carbonate (DMC) (volume ratio, 1:1:1) with 1 mol/L LiPF₆. The electrode performance was characterized by cyclic voltammetry (CV), galvanostatic charge–discharge, and electrochemical impedance spectroscopy (EIS), respectively. These tests were performed on the Land automatic battery tester (Wuhan, China) and electrochemical workstation (CHI604E and IM6ex, China). The test parameters were as follows, in regard of galvanostatic charge–discharge, $\varphi_{\text{initial}}=3.0$ V (vs Li/Li⁺), $\varphi_{\text{end}}=0.01$ V (vs Li/Li⁺), with respect to CV, voltage range 0.01–3.0 V (vs Li/Li⁺), scan rate 0.1 mV/s, as for EIS, frequency range 100 kHz–10 mHz, scan rate 0.5 mV/s. The specific capacity for the Si/TiO₂/CFs composite is derived upon the total mass of the composite.

3 Results and discussion

3.1 Phase structure and chemical component analysis

Figure 2(a) displays XRD patterns of commercial Si nanoparticles, Si/TiO₂, Si/CFs, and Si/TiO₂/CFs composites. The dominant peaks located at 2θ values of 56.1° , 47.3° , and 28.4° are corresponding to the (311),

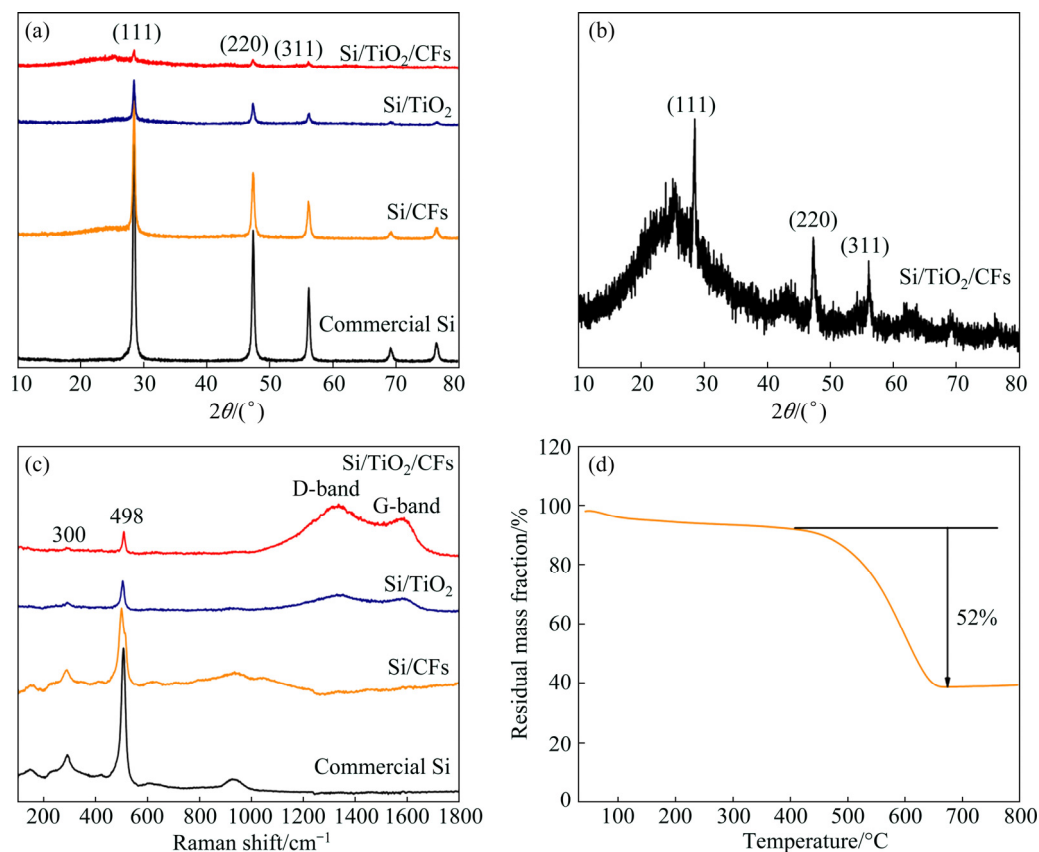


Fig. 2 Phase structure and chemical component analysis of commercial Si, Si/TiO₂, Si/CFs, and Si/TiO₂/CFs composites: (a, b) XRD patterns; (c) Raman spectra; (d) TG curve

(220), and (110) planes of crystalline Si (JCPDS No. 77–2107). For the commercial Si sample, the peak is relatively sharp owing to the aggregation of nanoparticles. The peak intensity of Si/TiO₂/CFs composite is the lowest as a result of the double-coating of TiO₂ and carbon fiber. As illustrated in Fig. 2(b), the broad peak located at 2θ of 25° is corresponding to the overlapping of anatase TiO₂ [19] and carbon fibers [20], which can also be detected in Si/TiO₂ and Si/CFs composites. Raman spectra of four samples are illustrated in Fig. 2(c) to verify the lattice vibration mode of composites. The vibration modes at 300 and 495 cm⁻¹ are owing to the vibration of the crystalline Si. The bands at 1360 and 1580 cm⁻¹ on the spectra of Si/CFs and Si/TiO₂/CFs composites are clearly indexed to the characteristic bands of graphene, that is, D-band and G-band. The intensity ratios (I_D/I_G) of Si/CFs and Si/TiO₂/CFs composites are calculated as 1.11 and 1.20, respectively. This result shows the partial graphitizing of the carbon matrix that will improve the electron transportation of the composite. Meanwhile, both D- and G-bands are wide peaks, indicating that CFs has a short-range disordered graphite structure [21]. The band at 498 cm⁻¹ of Si/TiO₂ and Si/TiO₂/CFs composites has a slight offset, which may be caused by the superposition of the characteristic bands of anatase TiO₂ [22]. Moreover, the carbon content of Si/TiO₂/CFs composite

is 52% according to the TG curve (Fig. 2(d)). It is assumed that there is no loss of Si during the whole synthesis process of the Si/TiO₂/CFs composite (since losses are avoided as far as possible in the process of collecting products in each step). Therefore, the Si content can be estimated by the data recorded in each step. The mass fractions of Si and TiO₂ in the Si/TiO₂/CFs composite are approximately 22% and 26%, respectively.

3.2 Morphology and microstructure

Figure 3 illustrates the detailed nanostructure of Si/TiO₂/CFs composite. It can be seen from the TEM images that the majority of the Si/TiO₂ particles are covered by carbon fibers, and the particles are evenly dispersed without obvious agglomeration (Fig. 3(a)). Most carbon fibers reported to improve electrochemical and mechanical stability of the silicon-based anode are limited on nanometer scale, 100–500 nm [5,23,24]. Thus, the silicon nanoparticles are prone to be exposed on the surface of nanofiber after carbonated shrinkage of carbon matrix, resulting in the crush and pulverization of active silicon. Therefore, the diameter of Si/TiO₂/CFs composite prepared in this work is controlled on the micrometer scale, the silicon nanoparticles are encapsulated by carbon fibers to effectively improve the cycling stability of electrode materials. EDS is utilized to

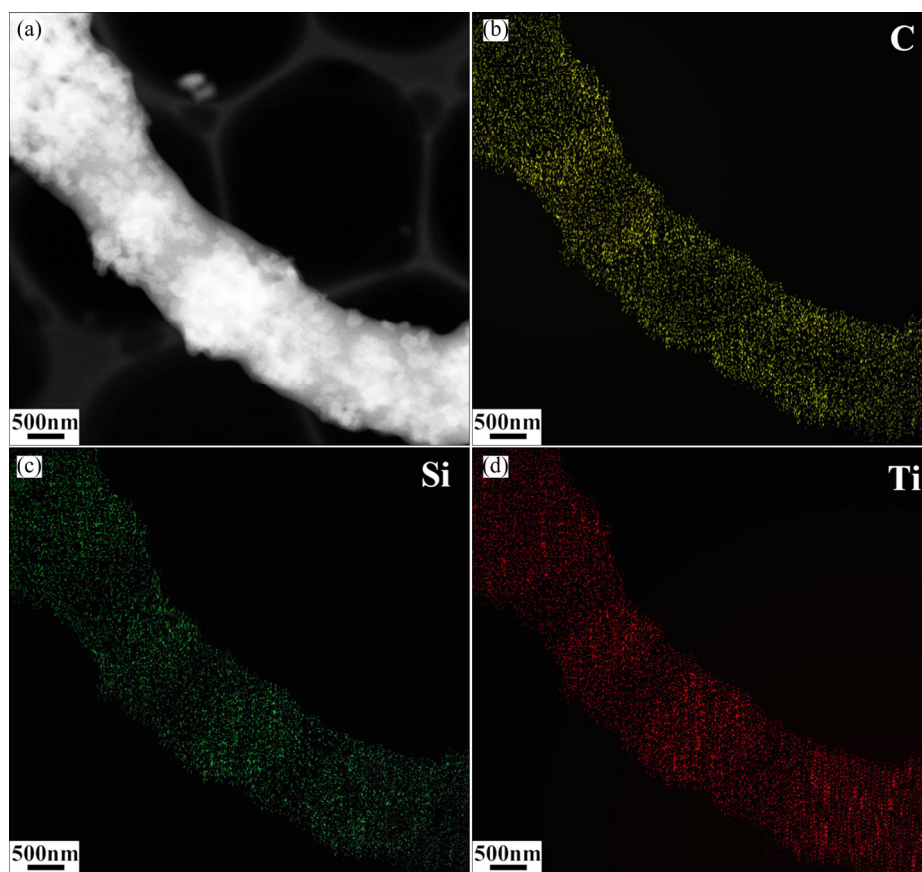


Fig. 3 TEM image of Si/TiO₂/CFs composite (a), and EDS images of C (b), Si(c) and Ti(d) elements

further illustrate the distribution of Si, Ti and C in the prepared Si/TiO₂/CFs composite. As illustrated in Figs. 3(b–d), three elements Si, Ti and C are uniformly distributed in the composite, indicating that the Si/TiO₂ particles are homogeneously coated by porous carbon fibers.

Figure 4 displays the morphology changes of the commercial Si and Si/TiO₂/CFs composite at different statuses. As shown in Fig. 4(a), the commercial Si powders are subspherical particles with a diameter of 30–50 nm. The Si/TiO₂/CFs composite is prepared through a sol–gel method followed by an electrospinning and carbonization process. Figures 4(b–d) show the morphologies of the composite at different statuses, i.e., as-spun, stabilized and carbonized statuses. The as-spun fibers are smooth and anisotropic, with a diameter of about 1.5 μm. The spinning fibers are arranged in the same direction with less staggered distribution, indicating that the operating voltage is stable in the process of electrospinning. After being stabilized at 250 °C for 2 h, the morphology of carbon fibers remains the same, not bent and staggered arrangement. As for the carbonized ones, in which PAN gets rid of the small

molecule gas such as CO₂ in high-temperature calcination, composite fibers get through bending and contraction, then present porous structure and staggered arrangement. Such porous and staggered configuration is beneficial to forming a connected channel and improving the electrical conductivity of the anode materials. At the same time, the surface of the carbonized fibers becomes rough, with a few Si/TiO₂ particles exposed.

3.3 Electrochemical performance

The lithium storage of silicon-based materials is based on the alloying mechanism. If silicon is completely lithiated into Li_{4.4}Si, it has a specific capacity as 4200 mA·h/g. To further explore the structural advantages of the Si/TiO₂/CFs composite as an alternative electrode material of Li-ion batteries, electrochemical tests are conducted. CV curves of Si/TiO₂/CFs electrode are used to determine the reaction and the reversibility (Fig. 5(a)). In the first discharge process, the broad reduction peak located at 0.5–0.7 V is owing to the generation of the SEI film. The reduction peak located at 0.2 V represents the change from polycrystalline silicon into amorphous Li_xSi alloy. In

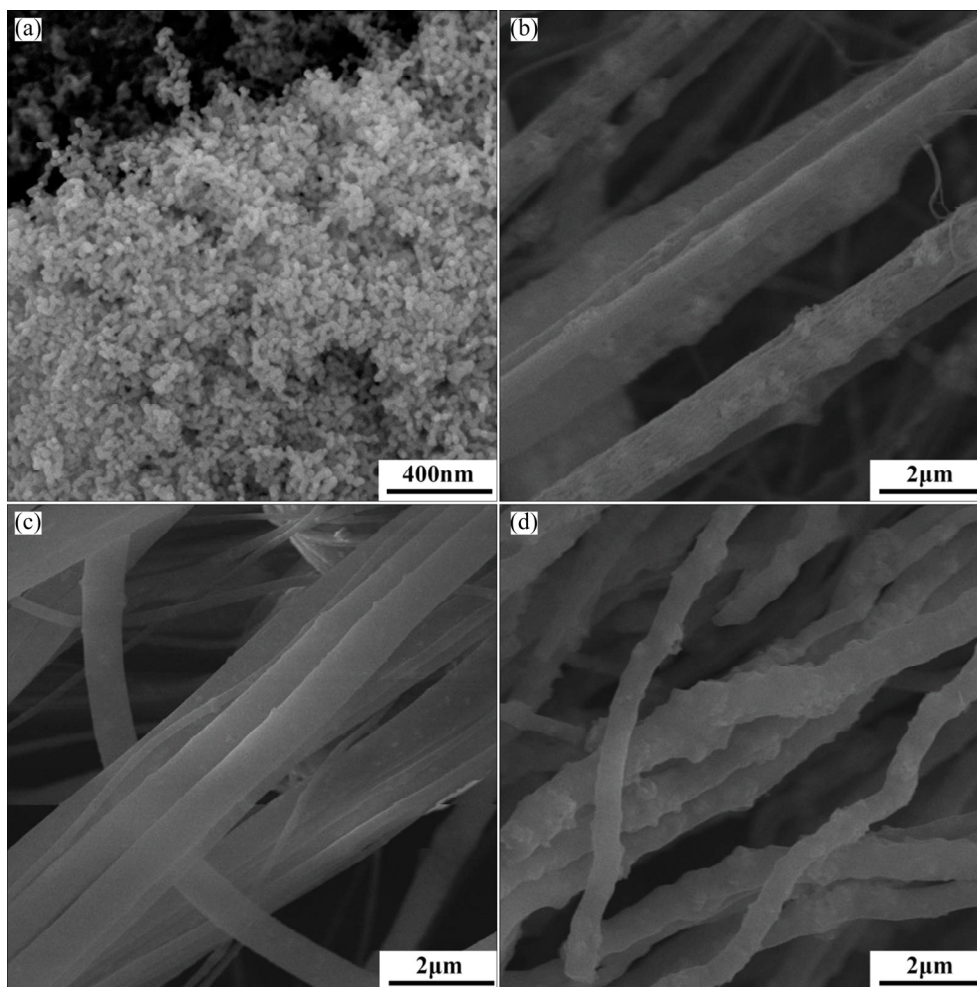


Fig. 4 SEM images of commercial Si (a) and Si/TiO₂/CFs composite at as-spun (b), stabilized (c) and carbonized (d) statuses

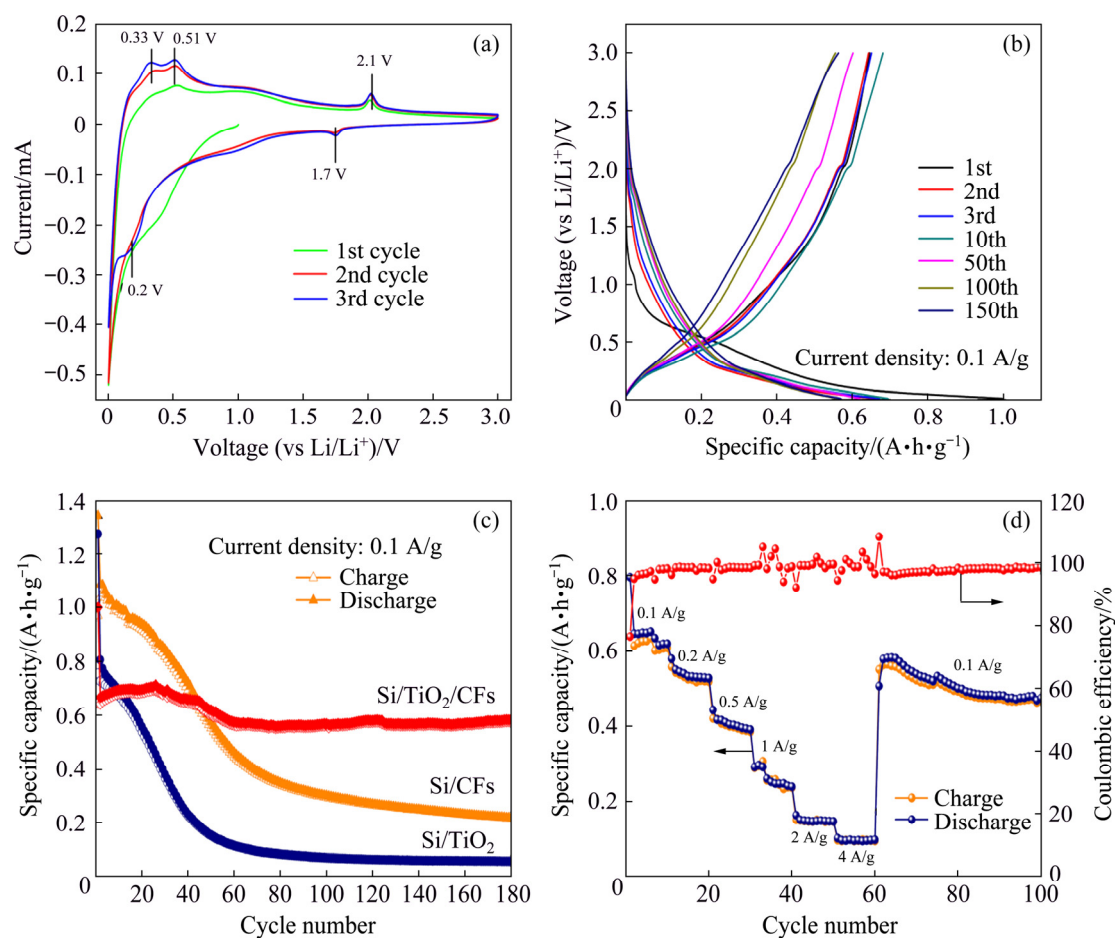


Fig. 5 Electrochemical performances of Si/TiO₂, and Si/CFs, Si/TiO₂/CFs composites: (a) CV curves; (b) Charge–discharge profiles; (c) Galvanostatic charge–discharge properties; (d) Bate capability

addition, the sharp peak located at 0.04 V corresponds to the rapid transformation of Li_xSi to Li₁₅Si₄ [25]. In the subsequent charge process, the oxidation peaks at 0.33 and 0.51 V are indexed to the delithiation from Li₁₅Si₄ to Li_xSi and Li_xSi to Si. The reduction peak at 1.71 V and the oxidation peak at 2.12 V are corresponding to the lithiation–delithiation processes of the anatase TiO₂. The high coincidence of CV curves after the first loop also indicates the excellent reversibility of the Si/TiO₂/CFs electrode. Moreover, the area of the CV curve increases slightly as a result of the continuous activation of the anode material. As displayed in the galvanostatic charge–discharge voltage profiles (Fig. 5(b)) under a current density of 0.1 A/g, the voltage change of the Si/TiO₂/CFs composite electrode is consistent with the CV curves. In detail, the voltage platforms at 0.2 and 0.5 V are indexed to the lithiation–delithiation process of Li_xSi alloys, while those at 1.7 and 2.1 V are indexed to the charge–discharge of TiO₂. The high overlapping after 10 cycles also proves the superior reversibility of the Si/TiO₂/CFs composite electrode. The galvanostatic charge–discharge tests are then utilized to compare the lithium storage capacity of

Si/TiO₂, Si/CFs and Si/TiO₂/CFs composites (Fig. 5(c)). The first discharge capacities of Si/TiO₂, Si/CFs and Si/TiO₂/CFs composites are 1275.8, 1343.9 and 999.8 mA·h/g under a current density of 0.1 A/g, with the corresponding coulombic efficiencies of 49.2%, 72.1% and 64.7%, respectively. The relatively low first-cycle coulombic efficiencies of the ones coated with TiO₂ are due to the slow activation of TiO₂ [26]. In the subsequent cycling process, the performance of the Si/TiO₂ electrode decays quickly for the low conductivity. In contrast, the specific capacity of Si/CFs composite shows relatively slow attenuation due to the constraint effect of carbon fibers at the micrometer scale. Under the dual-restriction of carbon fibers and TiO₂, the Si/TiO₂/CFs electrode performs stably. The discharge specific capacities of three electrodes are 56.1, 271.2 and 583.4 mA·h/g under a current density of 0.1 A/g after 180 cycles, and the corresponding capacity retentions are 6.9%, 30%, and 87.4% from the second cycle onwards, respectively. It is believed that the decay of capacity is related to the powder pulverization caused by the volume expansion during the charge–discharge process [27]. Therefore, the rigid TiO₂ and resilient carbon fiber coatings effectively

relieve the volume expansion of nano silicon and simultaneously improve the conductivity to enhance the cycling stability. Furthermore, Si/TiO₂/CFs electrode displays excellent rate performance under different current densities. As demonstrated in Fig. 5(d), the average specific capacities of the Si/TiO₂/CFs electrode are 635.9, 539.1, 407.4, 261.5, 148.7 and 95.7 mA·h/g under various current densities of 0.1, 0.2, 0.5, 1, 2 and 4 A/g, and the corresponding capacity retentions are 98.5%, 82.9%, 63.1%, 40.5%, 23% and 14.8% from the second cycle onwards, respectively. When the current density comes back to 0.1 A/g, a stable specific capacity of 522 mA·h/g is recovered.

In addition, Si/TiO₂/CFs electrode exhibits good stability in the long-term cycling under a current density of 1 A/g (Fig. 6). The first charge and discharge capacities of the composite electrode are 384.6 and 755.7 mA·h/g, respectively. Even after 900 cycles, the Si/TiO₂/CFs electrode has a reversible capacity of 351.3 mA·h/g, with a capacity retention of 92%. Overall, the Si/TiO₂/CFs anode presents a decent lithium storage capacity and superior cycling stability.

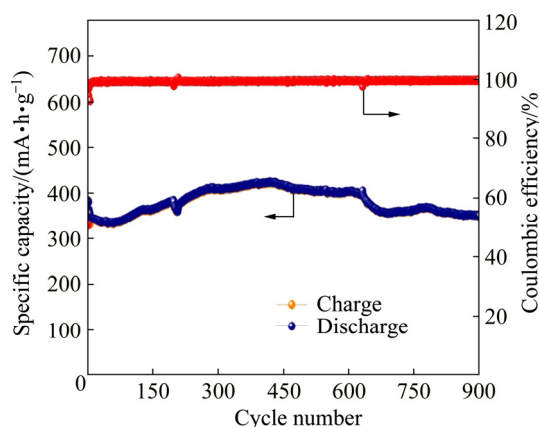


Fig. 6 Long-term charge–discharge performance of Si/TiO₂/CFs composite at current density of 1 A/g

Electrochemical impedance spectroscopy (EIS) is also used to evaluate the conductivity and diffusion property of Si/TiO₂/CFs composite electrode (Fig. 7). The impedance of four cells is composed of a semicircle in the high-frequency region and a straight line in the low-frequency region. In the low-frequency region, four samples have similar Warburg impedance (R_w) for the same electrolyte. Si/TiO₂ and Si/CFs electrodes have smaller charge transfer impedance (R_{ct} , about 120 Ω) compared with commercial silicon powder (about 165 Ω), suggesting that anatase TiO₂ and carbon fibers improve the electrical conductivity of the electrode materials. Therefore, the Si/TiO₂/CFs electrode exhibits the minimum R_{ct} (about 70 Ω), that is, the optimal conductivity and the rapid solid-state ion transmission rate.

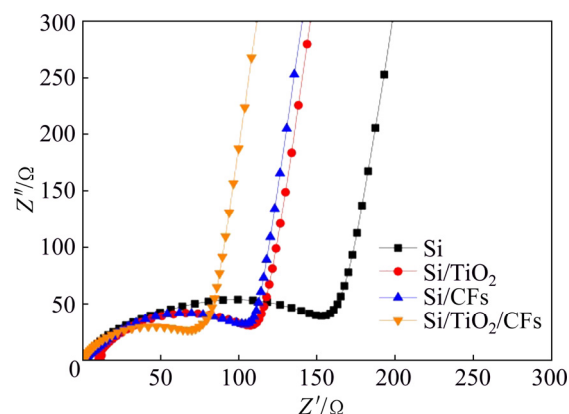


Fig. 7 Nyquist diagrams of commercial Si, Si/TiO₂, Si/CFs and Si/TiO₂/CFs composites

4 Conclusions

(1) A simple sol–gel method followed by an electrospinning process and high-temperature carbonization was utilized to synthesize the dual-shell Si/TiO₂/CFs composite.

(2) The carbonized composite is composed of staggered carbon fibers with a diameter of about 1.5 μm and encapsulating Si/TiO₂ particles, in which the Si, Ti and C elements uniformly distribute in the composite fibers.

(3) Unique fibrous structure and high conductivity make the Si/TiO₂/CFs composite obtain a superior reversible specific capacity (583.4 mA·h/g) and capacity retention (87.4%) after 180 cycles under the current density of 0.1 A/g, and as the current density ranges from 0.1 to 4 A/g, its specific capacity decreases from 635.9 to 95.7 mA·h/g. When the current density returns to 0.1 A/g, the specific capacity returns to 522 mA·h/g.

References

- [1] ZHENG Jun-chao, YANG Zhuo, WANG Peng-bo, TANG Lin-bo, AN Chang-sheng, HE Zhen-jiang. Multiple linkage modification of lithium-rich layered oxide Li_{1.2}Mn_{0.54}Ni_{0.13}Co_{0.13}O₂ for lithium ion battery [J]. ACS Applied Materials & Interfaces, 2018, 10(37): 31324–31329.
- [2] CHEN Qi-chao, YAN Guan-jie, LUO Li-ming, CHEN Fei, XIE Tang-feng, DAI Shi-can, YUAN Ming-liang. Enhanced cycling stability of Mg–F co-modified LiNi_{0.6}Co_{0.2}Mn_{0.2-y}MgyO_{2-z}F_z for Li-ion batteries [J]. Transactions of Nonferrous Metals Society of China, 2018, 28(7): 1397–1403.
- [3] OU Jun-ke, YANG Lin, ZHANG Zhen. Chrysanthemum derived hierarchically porous nitrogen-doped carbon as high performance anode material for lithium/sodium ion batteries [J]. Powder Technology, 2019, 344: 89–95.
- [4] ZHANG Bao-ping, XIA Guang-lin, CHEN Wei, GU Qin-fen, SUN Da-lin, YU Xue-bin. Controlled-size hollow magnesium sulfide nanocrystals anchored on graphene for advanced lithium storage [J]. ACS Nano, 2018, 12(12): 12741–12750.
- [5] SHOORIDEH G, KO B, BERRY A, DIVVLA M J, KIM Y S, LI Z, PATEL B, CHAKRAPANI S, JOO Y L. Harvesting interconductivity

- and intraconductivity of graphene nanoribbons for a directly deposited, high-rate silicon-based anode for Li-ion batteries [J]. *ACS Applied Energy Materials*, 2018, 1(3): 1106–1115.
- [6] LUO Wei, CHEN Xin-qí, XIA Yuan, CHEN Miao, WANG Lian-jun, WANG Qing-qing, LI Wei, YANG Jian-ping. Surface and interface engineering of silicon-based anode materials for Li-ion batteries [J]. *Advanced Energy Materials*, 2017, 8(29): 1701083.
- [7] LIU Rui-ping, SHEN Chao, DONG Yue, QIN Jin-lei, WANG Qi, IOCOZZIA J, ZHAO Shi-qiang, YUAN Kun-jie, HAN Cui-ping, LI Bao-hua, LIN Zhi-qun. Sandwich-like CNTs/Si/C nanotubes as high performance anode materials for Li-ion batteries [J]. *Journal of Materials Chemistry A*, 2018, 6(30): 14797–14804.
- [8] HE Ting, FENG Jian-ruí, ZHANG Yan, ZU Lian-hai, WANG Gui-chang, YU Yan, YANG Jin-hu. Stress-relieved nanowires by silicon substitution for high-capacity and stable lithium storage [J]. *Advanced Energy Materials*, 2018, 8(14): 1702805.
- [9] CHEN Qing-ze, ZHU Run-liang, LIU Shao-hong, WU Ding-cai, FU Hao-yang, ZHU Jian-xi, HE Hong-ping. Self-templating synthesis of silicon nanorods from natural sepiolite for high-performance Li-ion battery anodes [J]. *Journal of Materials Chemistry A*, 2018, 6(15): 6356–6362.
- [10] ZHANG Wei-ming, HU Jin-song, GUO Yu-guo, ZHENG Shu-fa, ZHONG Liang-shu, SONG Wei-guo, WAN Li-jun. Tin-nanoparticles encapsulated in elastic hollow carbon spheres for high-performance anode material in Li-ion batteries [J]. *Advanced Materials*, 2008, 20(6): 1160–1165.
- [11] WANG Jia-qing, YU Yan, GU Lin, WANG Chun-lei, TANG Kun, MAIER J. Highly reversible lithium storage in Si (core)-hollow carbon nanofibers (sheath) nanocomposites [J]. *Nanoscale*, 2013, 5(7): 2647–2650.
- [12] YOON T, BOK T, KIM C, NA Y, PARK S, KIM K S. Mesoporous silicon hollow nanocubes derived from metal-organic framework template for advanced Li-ion battery anode [J]. *ACS Nano*, 2017, 11(5): 4808–4815.
- [13] MA Tian-yi, YU Xiang-nan, CHENG Xiao-lu, LI Hui-yu, ZHU Wen-tao, QIU Xin-ping. Confined solid electrolyte interphase growth space with solid polymer electrolyte in hollow structured silicon anode for Li-ion batteries [J]. *ACS Applied Materials & Interfaces*, 2017, 9(15): 13247–13254.
- [14] FANG Shan, SHEN Lai-fa, XU Gui-yin, NIE Ping, WANG Jie, DOU Hui, ZHANG Xiaogang. Rational design of void-involved Si@TiO₂ nanospheres as high-performance anode material for Li-ion batteries [J]. *ACS Applied Materials & Interfaces*, 2014, 6(9): 6497–6503.
- [15] KIM J W, RYU J H, LEE K T, OH S M. Improvement of silicon powder negative electrodes by copper electroless deposition for lithium secondary batteries [J]. *Journal of Power Sources*, 2005, 147(1–2): 227–233.
- [16] KO M, CHAE S, JEONG S, OH P, CHO J. Elastic α -silicon nanoparticle backboned graphene hybrid as a self-compacting anode for high-rate lithium ion batteries [J]. *ACS Nano*, 2014, 8(8): 8591–8599.
- [17] CHEN S, SHEN L, AKEN P A V, MAIER J, YU Y. Dual-functionalized double carbon shells coated silicon nanoparticles for high performance Li-ion batteries [J]. *Advanced Materials*, 2017, 29(21): 1605650.
- [18] WU H, CHAN G, CHOI J W, RYU I, YAO Y, MCDOWELL M T, LEE S W, JACKSON A, YANG Y, HU L B, CUI Y. Stable cycling of double-walled silicon nanotube battery anodes through solid-electrolyte interphase control [J]. *Nature Nanotechnology*, 2012, 7(5): 309–314.
- [19] LUO Wei, WANG Yun-xiao, WANG Lian-jun, JIANG Wan, CHOU S, DOU Shi-xue, LIU Hua-kun, YANG Jian-ping. Silicon/mesoporous carbon/crystalline TiO₂ nanoparticles for highly stable lithium storage [J]. *ACS Nano*, 2016, 10(11): 10524–10532.
- [20] KIM S Y, YANG K S, KIM B H. Improving the microstructure and electrochemical performance of carbon nanofibers containing graphene-wrapped silicon nanoparticles as a Li-ion battery anode [J]. *Journal of Power Sources*, 2015, 273: 404–412.
- [21] WANG Hong-kang, YANG Xu-ming, WU Qi-zhen, ZHANG Qiao-bao, CHEN Hui-xin, JING Hong-mei, WANG Jin-kai, MI S B, ROGACH A L, NIU Chun-ming. Encapsulating silica/antimony into porous electrospun carbon nanofibers with robust structure stability for high-efficiency lithium storage [J]. *ACS Nano*, 2018, 12(4): 3406–3416.
- [22] KELLY S, POLLAK F H, TOMKIEWICZ M. Raman spectroscopy as a morphological probe for TiO₂ aerogels [J]. *The Journal of Physical Chemistry B*, 1997, 101: 2730–2734.
- [23] AN G, KIM H, AHN H. Improved ionic diffusion through the mesoporous carbon skin on silicon nanoparticles embedded in carbon for ultrafast lithium storage [J]. *ACS Applied Materials & Interfaces*, 2018, 10(7): 6235–6244.
- [24] CHEN Yan-li, HU Yi, SHEN Zhen, CHEN Renzhong, HE Xia, ZHANG Xiang-wu, LI Yong-qiang, WU Ke-shi. Hollow core-shell structured silicon@carbon nanoparticles embed in carbon nanofibers as binder-free anodes for Li-ion batteries [J]. *Journal of Power Sources*, 2017, 342: 467–475.
- [25] LIANG Ge-meng, QIN Xian-ying, ZOU Jin-shuo, LUO Lai-yan, WANG Yun-zhe, WU Meng-yao, ZHU Hua, CHEN Guo-hua, KANG Fei-yu, LI Bao-hua. Electrospun silicon-embedded porous carbon microspheres as Li-ion battery anodes with exceptional rate capacities [J]. *Carbon*, 2018, 127: 424–431.
- [26] WANG Xiao-yan, FAN Ling, GONG De-cai, ZHU Jian, ZHANG Qing-feng, LU Bing-an. Core-shell Ge@graphene@TiO₂ nanofibers as a high-capacity and cycle-stable anode for lithium and sodium ion battery [J]. *Advanced Functional Materials*, 2016, 26(7): 1104–1111.
- [27] POMERANTSEVA E, GOGOTSI Y. Two-dimensional heterostructures for energy storage [J]. *Nature Energy*, 2017, 2(7): 17089.

双壳层 Si/TiO₂/CFs 复合物的制备及其储锂性能

曾婧^{1,2}, 彭超群¹, 王日初^{1,2}, 刘雅敬^{1,2}, 王小锋^{1,2}, 刘军¹

1. 中南大学 材料科学与工程学院, 长沙 410083; 2. 湖南省电子封装与先进功能材料重点实验室, 长沙 410083

摘要: 针对硅基阳极在循环过程中体积变化大、SEI膜不稳定、电子电导率和离子电导率低等固有缺陷, 采用简单方法合成双壳层 Si/TiO₂/CFs 复合材料。内部刚性 TiO₂ 壳层可缓解锂化脱锂过程中纳米硅的巨大体积膨胀, 外部弹性碳纤维壳层的交错多孔结构有利于电子和离子的快速传输。该方法制备的 Si/TiO₂/CFs 复合材料具有优异的可逆比容量(583.4 mA·h/g)、高倍率性能和良好的循环性能。这种双壳层包覆方法亦可用于合成在循环过程中具有较大体积变化的其他电极材料。

关键词: 双壳层; 硅阳极; 静电纺丝; 溶胶凝胶法; 锂离子电池